24 May 2002

Chemical Physics Letters 358 (2002) 51–56

CHEMICAL PHYSICS LETTERS

www.elsevier.com/locate/cplett

Probing a colored-noise induced peak of a strongly damped Brownian system by one- and two-dimensional spectroscopy

Yoko Suzuki *, Yoshitaka Tanimura

Institute for Molecular Science, Myodaiji, Okazaki 444-8585, Japan

Received 28 February 2002; in final form 28 March 2002

Abstract

When dynamics of a system strongly coupled to a white-noise environment is overdamped, in linear spectroscopy, the spectrum is observed as one peak near zero vibrational frequency. We found, however, that if the noise induced by the environment is colored and its correlation time is long, there is an additional peak at a frequency different from the system. We study the multi-dimensional spectrum, to observe the interplay between the overdamped motion and the weakly damped motion induced by the colored noise. Finally, we discuss the connection between the peak due to the colored noise and the Boson peak found in glass materials and supercooled liquids.

Dissipations play a central role in dynamics of a system in the condensed phases. This problem is most commonly studied by the Brownian oscillator Hamiltonian given by [1–3]

$$H = \frac{P^2}{2M} + \frac{M\Omega^2 Q^2}{2} + \sum_i \left[\frac{p_i^2}{2m_i} + \frac{m_i\omega_i^2}{2}(x_i - Q)^2 \right]. \tag{1}$$

Here, Q, P, M, and x_i, p_i, m_i denote the coordinate, conjugate momentum, mass of the system and the ith bath oscillator, respectively. The interaction between the system and the bath oscillators is expressed as $-\sum_i m_i\omega_i^2 x_i Q$. The character of the heat bath is described by the spectral distribution function defined by $I(\omega) \equiv \pi \sum_i (m_i\omega_i^3/2)\,\delta(\omega - \omega_i)$. The counter term $\sum_i m_i\omega_i^2 Q^2/2$ is introduced in Eq. (1) to keep the translational symmetry of the Hamiltonian for $\Omega \to 0$. If we neglect this term, the minimum of the potential surface of the whole system given by Hamiltonian (1) for Q is at $x_i = Q$ for all i. The 'effective' potential renormalized by the system–bath coupling is then given by $M\Omega^2 Q^2/2 - \sum_i c_i^2 Q^2/(2m_i\omega_i^2)$, which causes a negative shift $(\Delta\omega)^2 = -\sum_i c_i^2/(Mm_i\omega_i^2)$ in the squared frequency Ω^2. Since such coupling-induced renormalization effects can be very large, they strongly deform the potential. The counter term compensates such deformation.

The molecular vibration in solvated molecules is described by Hamiltonian (1), in which the system

* Corresponding author. Fax: +11-81-53-4660.
E-mail address: youko@ims.ac.jp (Y. Suzuki).

0009-2614/02/$ - see front matter
PII: S0009-2614(02)00563-8

corresponds to the inter- and intra-molecular vibrations interacting with a bath of the inter-molecular one. In vibrational Raman spectroscopy, dynamics of the system is probed by a correlation function of the Raman polarizability $\alpha(Q)$. The third-order Raman response is defined by the two-body correlation function as $R^{(3)}_{\mathrm{Raman}}(t) = \langle[\alpha(Q(t)), \alpha(Q(0))]\rangle \approx \alpha_1^2\langle[Q(t), Q(0)]\rangle$ for the polarizability approximated by $\alpha(Q) = \alpha_1 Q + \alpha_2 Q^2/2 + \cdots$. As for the spectral distribution function, we consider the Ohmic dissipation with Lorentzian cutoff, $I(\omega) = M\omega\gamma\omega_{\mathrm{D}}^2/(\omega^2 + \omega_{\mathrm{D}}^2)$, which induces the colored noise in the exponentially decaying form of the dissipation kernel $\eta(t) = M\gamma\omega_{\mathrm{D}} \times \exp(-\omega_{\mathrm{D}}t)$, where γ and ω_{D} are the damping strength and the cutoff frequency [4]. The third-order Raman response is then expressed as [5]

$$R^{(3)}_{\mathrm{Raman}}(t) = \alpha_1^2 C(t), \tag{2}$$

where the function $C(t) \equiv (\mathrm{i}/\hbar)\mathrm{Tr}(\mathrm{e}^{-\beta H}[Q(t), Q(0)])/\mathrm{Tr}\,\mathrm{e}^{-\beta H}$ is expressed in terms of the inverse Laplace transform as [1,2]

$$C(t) = \oint_{C_z} \frac{\mathrm{d}z}{2\pi\mathrm{i}} \frac{\mathrm{e}^{zt}}{M[z^2 + z\gamma\omega_{\mathrm{D}}/(\omega_{\mathrm{D}} + z) + \Omega^2]}. \tag{3}$$

The above result has been well-known. However we found interesting effects for strong system–bath coupling, in which the system usually does not show any characteristic motion, if the noise correlation time is much longer than the time scale of the system's motion. To demonstrate this point, in Fig. 1 we plot the imaginary part of the Fourier transformed response function $R^{(3)}(\omega) = \int_0^\infty \mathrm{d}T \exp(\mathrm{i}\omega T)R^{(3)}(T)$ for very large system–bath coupling $\gamma/\Omega = 100$ for different cutoff frequencies; $\omega_{\mathrm{D}}/\Omega = \infty$, i.e., Gaussian-white limit (solid line), $\omega_{\mathrm{D}}/\Omega = 0.6$ (dashed line), and $\omega_{\mathrm{D}}/\Omega = 0.1$ (dotted line). Here, we set the system oscillator frequency to $\Omega = 100\ \mathrm{cm}^{-1}$ which is the typical value for inter-molecular vibrational motion. Since we choose strong system–bath coupling, it is expected that the system motion is overdamped. Fig. 1 shows that, in the Gaussian-white case (solid line), such a motion is observed in the spectrum as a featureless peak near zero frequency. In the case of the colored noise, dashed line and dotted one, however, an additional peak appears which is different from the resonant frequency position Ω.

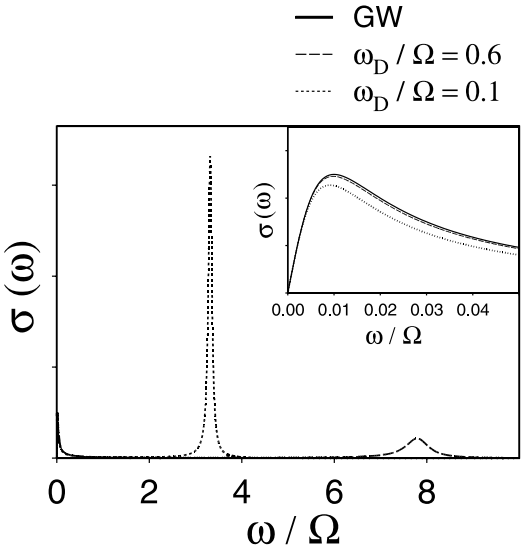

Fig. 1. The absorption spectrum of the damped harmonic oscillator for the different cutoff frequency; $\omega_{\mathrm{D}}/\Omega = \infty$, i.e., the Gaussian-white (GW) limit (solid line), $\omega_{\mathrm{D}}/\Omega = 0.6$ (dashed line), and $\omega_{\mathrm{D}}/\Omega = 0.1$ (dotted line). The harmonic oscillator frequency and the damping constant are set as $\Omega = 100\ \mathrm{cm}^{-1}$ and $\gamma/\Omega = 100$, respectively. The inset depicts the spectrum around zero frequency.

In contrast to the Gaussian-white case, this peak remains as long as the coupling strength is strong and ω_{D} is very small. The peak shifts to the blue for larger ω_{D} (the dashed and dotted lines of Fig. 1) or γ (not shown).

The origin of this peak can be understood as follows: in the slow modulation case ($\omega_{\mathrm{D}} \sim 0$), the frequency ω_i is distributed in the narrow range around $\omega_i \sim 0$ ($\omega_i \neq 0$), so that x_i and p_i are represented as a typical oscillator coordinate and momentum which we denote as x_0 and p_0. By using the relation, $\int_0^\infty \mathrm{d}\omega I(\omega)/(\pi\omega) = \sum_i m_i\omega_i^2/2 = M\gamma\omega_{\mathrm{D}}/2$, the Hamiltonian (1) is approximated by the two coupled oscillators:

$$H \sim \frac{P^2}{2M} + \frac{M}{2}(\Omega^2 + \gamma\omega_{\mathrm{D}})Q^2 + \frac{p_0^2}{2\bar{m}} + \frac{\bar{m}\bar{\omega}^2 x_0^2}{2} - M\gamma\omega_{\mathrm{D}}x_0 Q, \tag{4}$$

where $\bar{m} = 1/[\sum_i (1/m_i)]$ and $\bar{\omega} = \sqrt{M\gamma\omega_{\mathrm{D}}/\bar{m}}$. The Hamiltonian (4) is then diagonalized as

$$H \sim \sum_{i=\pm} \left(\frac{p_i^2}{4A\bar{m}M} + (A\bar{m}M)\lambda_i^2 y_i^2 \right), \tag{5}$$

where $y_\pm$ and $p_\pm$ are the normal coordinates and the conjugate momentum for the eigenfrequencies

$$(\lambda_\pm)^2 = \frac{1}{2}\left[(\bar{\Omega}^2 + \bar{\omega}^2) \pm \sqrt{(\bar{\Omega}^2 - \bar{\omega}^2)^2 + 4\gamma\omega_D\bar{\omega}^2}\right], \tag{6}$$

and we set $\bar{\Omega}^2 = \Omega^2 + \gamma\omega_D$ and $A^2 = (\bar{\Omega}^2 - \bar{\omega}^2)^2 + 4\gamma\omega_D\bar{\omega}^2$. The correlation function $C(t)$ is then approximated by

$$C(t) \sim \frac{1}{2AM}\left[\frac{A+B}{\lambda_+}\sin(\lambda_+ t) + \frac{A-B}{\lambda_-}\sin(\lambda_- t)\right], \tag{7}$$

where we set $B = \bar{\Omega}^2 - \bar{\omega}^2$.

For $\bar{\omega}/\bar{\Omega} \ll 1$, the normal mode frequencies are given by $\lambda_+ \sim \bar{\Omega}$ and $\lambda_- \sim 0$. If we consider the strong coupling case $\gamma\omega_D \gg \Omega^2$, then we have the peaks of '+' and '−' modes at $\omega \sim \sqrt{\gamma\omega_D}$ and 0, respectively. From the above derivation, the origin of the additional peak is attributed to a single mode of the heat-bath, which is induced by the narrow band spectral distribution. The dynamics of the system play a minor role. Indeed, as indicated by Eq. (6), we observe this additional peak even in a free particle case ($\Omega \to 0$). To explore the origin of the peak in more detail, we consider the classical Langevin equation for an exponentially decaying noise given by

$$M\frac{d^2Q(t)}{dt^2} + \int_{t_I}^{t} dt'\eta(t-t')\frac{dQ(t')}{dt'} + \frac{\partial U(Q(t))}{\partial Q(t)} = R(t). \tag{8}$$

Here, $R(t)$ is the random fluctuation, which relates to the dissipation kernel as $\eta(t) = \langle R(t)R(0)\rangle = M\gamma\omega_D \exp(-\omega_D t)$. After integrated in part, the second term in the LHS of Eq. (8) leads to the equation of motion in the form

$$M\frac{d^2Q(t)}{dt^2} + M(\Omega^2 + \gamma\omega_D)Q(t) - M\gamma\omega_D e^{-\omega_D(t-t_I)}Q(t_I) = R(t), \tag{9}$$

where we neglected the term proportional to ω_D^2 by assuming ω_D is small. The second term of the LHS in Eq. (9) includes the additional potential term $M\gamma\omega_D Q^2/2$, which agrees with the counter term ($\int_0^\infty d\omega I(\omega)Q^2/(\pi\omega) = M\gamma\omega_D Q^2/2$) in the Hamiltonian (1). This additional term leads to a peak at the position $\sqrt{\gamma\omega_D}$ for $\gamma\omega_D \gg \Omega^2$, and can be regarded as the origin of the additional peak. Note that Eq. (8) has translational symmetry form for $\Omega \to 0$, whereas Eq. (9) does not. This is due to neglecting the term proportional to ω_D^2. This means that if the motion of the system decays much faster than the characteristic time scale of the bath oscillation ($\sqrt{M\gamma\omega_D/\bar{m}}$), the system cannot recover the translational symmetry. In such a case, the mechanism of the counter term to maintain the translational symmetry of the system is broken down and the counter term acts as the additional potential. The appearance of this additional peak is, therefore, an indication of the counter term. As can be seen from the form of Eq. (9), the peak position, which is determined by the second term in the LHS, shifts to the blue for larger ω_D. Thus, this peak vanishes in the Gaussian-white case with $\omega_D \to \infty$.

Although the additional peak presented here is the prominent feature of the present study, in a real experimental situation, it is not so easy to observe the difference between such a peak and other peaks with different origins. It is because the additional peak can be observed only in the condensed phases, where many molecular vibrational motions associated with large inhomogeneity play a role. In such a case, multi-dimensional spectroscopy, which measures the multi-body correlation functions of the polarizability or the dipole moment, can give an additional insight. Examples of the multi-dimensional vibrational techniques are the fifth- [6,7] and seventh-order Raman spectroscopies [8] and the second-order [9] and third-order infrared spectroscopies [10]. The seventh-order Raman and the third-order IR spectroscopies correspond to the Raman echo and the IR photon echo, respectively. We calculated the fifth-order 2D Raman and third-order 2D IR signals defined by

$$R^{(5)}_{\mathrm{Raman}}(T_2, T_1) = \langle[[[\alpha(Q(T_1+T_2)), \alpha(Q(T_1))], \alpha(Q)]\rangle$$

and

$$R^{(3)}_{\mathrm{IR}}(T_3, T_2, T_1) = \langle[[[[\mu(Q(T_1+T_2+T_3)), \mu(Q(T_1+T_2))], \mu(Q(T_1))], \mu(Q)]\rangle,$$

respectively, where $\mu(Q) = \mu_1 Q + \mu_2 Q^2/2 + \cdots$ is the dipole moment. Since the two results are

qualitatively similar, we present the third-order IR signal. Note that since we express $\alpha(Q)$ and $\mu(Q)$ in the power of Q, Nth-order IR spectroscopy is formally identical with the $(2N+1)$th-order Raman spectroscopy [11]. The present results therefore agree with the seventh-order 2D Raman results.

The third-order IR response function for the Brownian oscillator system is expressed as [11]

$$R^{(3)}_{\mathrm{IR}}(T_3, T_2 = 0, T_1) = 2\mu_1^2\mu_2^2 C(T_1)(C(T_3))^2, \qquad (10)$$

where T_i is the time interval between the ith and $i+1$th pairs of impulsive laser pulses, and we set $T_2 = 0$ to consider the situation of the IR photon echo experiments (see Fig. 2). The anti-symmetric correlation function $C(t)$ is defined by Eq. (7).

Fig. 3 shows the third-order IR response function in the frequency domain, which is defined by

$$I^{(3)}_{\mathrm{IR}}(\omega_3, \omega_1) = \left| \int_0^\infty \mathrm{d}T_1 \int_0^\infty \mathrm{d}T_3\, \mathrm{e}^{\mathrm{i}\omega_1 T_1 + \mathrm{i}\omega_3 T_3} R^{(3)}_{IR}(T_3, 0, T_1) \right|. \qquad (11)$$

Since the results are symmetrical with respect to the x and y axes, we depict the first quadrant of the 2D spectra, $I^{(3)}_{\mathrm{IR}}(\omega_3, \omega_1)$. The harmonic oscillator frequency and the damping constant are chosen as $\Omega = 100\ \mathrm{cm}^{-1}$ and $\gamma/\Omega = 100$, respectively. We set the cutoff frequency as $\omega_{\mathrm{D}}/\Omega = \infty$ in Fig. 3a i.e., Gaussian-white limit whereas $\omega_{\mathrm{D}}/\Omega = 0.1$ in Fig. 3b.

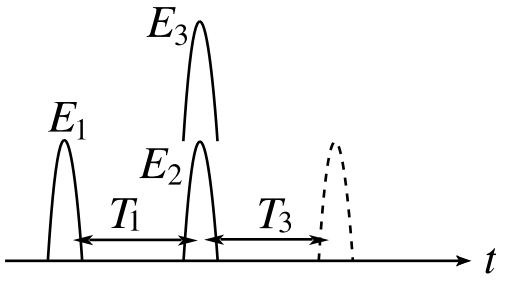

Fig. 2. Time sequence of the third-order IR experiments. The pulses labeled 1, 2, and 3 incident on the sample at time intervals T_1 between 1 and 2 and $T_2 = 0$ between 2 and 3. They create a third-order polarization illustrated by the dashed line in the sample for time T_3 after the third pulse. The third-order polarization is evaluated by the third-order response function.

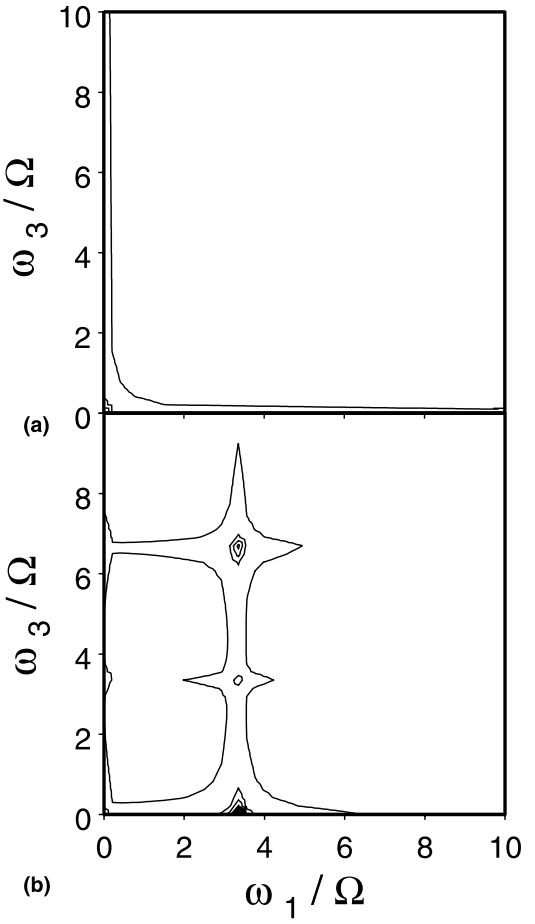

Fig. 3. Contour plot of the third-order IR response of the strongly damped harmonic oscillator in the frequency domain for the different cutoff frequency: (a) $\omega_{\mathrm{D}}/\Omega = \infty$, i.e., the Gaussian-white (GW) limit and (b) $\omega_{\mathrm{D}}/\Omega = 0.1$. The harmonic oscillator frequency and the damping constant are set as $\Omega = 100\ \mathrm{cm}^{-1}$ and $\gamma/\Omega = 100$, respectively. Since the results are symmetrical with respect to the x and y axes, we depict the first quadrant of the 2D spectra. In (b), the intensities of the peaks are $\sim$0.8 at $(\omega_1, \omega_3) = (\bar{\Omega}, 2\bar{\Omega})$, $\sim$0.05 at $(\omega_1, \omega_3) = (0, \bar{\Omega})$, $\sim$0.2 at $(\omega_1, \omega_3) = (\bar{\Omega}, \bar{\Omega})$ and $(0, 2\bar{\Omega})$, $\sim$1.6 at $(\omega_1, \omega_3) = (\Omega, 0)$, and $\sim$0.3 at $(\omega_1, \omega_3) = (0, 0)$.

The peak at $(\omega_1, \omega_3) = (0, 0)$ in Figs. 3a and b arises from the overdamped motion of the system oscillators. We find the additional peaks in the Gaussian–Markovian case in Fig. 3b.

Although here we consider a single mode system, the appearance of these peaks can be understood from the argument developed for a two-mode system [12]. It is because, as discussed in

the third-order case, an overdamped single-mode oscillator system coupled to the slow noise bath can be expressed by two uncoupled modes: one mode related to the system oscillator described by y_-, and the other mode related to the motion of the bath oscillators with the narrow frequency distribution described by y_+. Since the system coordinate is then expressed as $Q = c_+y_+ + c_-y_-$, where c_- and c_+ are constants, laser excitation with the dipole element $\mu(Q) = \mu_1 Q + \mu_2 Q^2/2$ causes the one- and two-vibrational excitation or deexcitation processes for the '+' and '−' mode, in addition to the cross excitation-deexcitation process between the two modes described by y_-y_+.

The third-order 2D IR experiment consists of a single excitation laser pulse at time $t = 0$ followed by two coincident pulses (mixing pulses) at time $t = T_1$. These pulses create various coherences in the '+' and '−' modes, which can be observed by the detection pulse at $t = T_1 + T_3$. The spectrum in the double Fourier space therefore depicts the coherence involved in the third-order IR process. For example, the peak at $(\omega_1, \omega_3) = (\bar{\Omega}, 2\bar{\Omega})$, where $\bar{\Omega} = 3.6$, corresponds to the coherent process of mode '+' that involves the coherence with $\bar{\Omega}$ in the time period T_1 and $2\bar{\Omega}$ in the time period T_3. The pronounced feature of this result is peaks at $(\bar{\Omega}, \bar{\Omega})$, $(0, \bar{\Omega})$, and $(0, 2\bar{\Omega})$: they appear since the dipole moment has the cross terms y_-y_+ indicating the coupling between two modes through the dipole moment. Since a system with two independent modes cannot show such cross peaks, one may distinguish the additional peak from the others caused by two independent modes.

In this Letter we show that, if the correlation time of a noise resource is much longer than the time scale of the system's motion, a Brownian system with a strong system–bath interaction causes a prominent peak in the third-order Raman spectrum in addition to featureless peak near the zero frequency, which originates from the overdamped motion of the system. This prominent peak arises if the motion of the system decays faster than the characteristic time scale of the bath oscillators, which is determined by the highly localized spectral distribution induced by the long-time noise correlation. The character of this prominent peak and the near zero frequency peak can be understood by employing the approximated Hamiltonian expressed by the two uncoupled harmonic modes: one mode related to the bath oscillators with narrow band spectral distribution and the other mode related to the overdamped system motion. By plotting the third-order 2D IR signal, we can see that these two modes are coupling through the dipole moment. We note that, if the system potential includes the anharmonicity, the two modes couple through such an anharmonic part.

In this study, we limit our analysis to the Brownian harmonic oscillator system with the Gaussian–Markovian noise bath, but similar behavior is seen for such a damped two-dimensional rotator system [13] and a Brownian system with non-linear system–bath coupling [14]. The similar peak may be seen in any damped system if the noise has a narrow band spectral distribution, e.g., that defined by the spectral distribution function with a power law form, $I(\omega) \propto \omega^s$.

Finally, we discuss the connection between the present study and the Boson peak, which was found in the low energy region (2–10 meV) of inelastic neutron or Raman scattering spectra in many glassy materials and some supercooled liquids, which are assumed to be the strongly damped environment [15–17]. The feature of the Boson peak is universal and does not depend on the investigated samples: its temperature dependence can be scaled by the Bose factor for vibrational excitation. Many attempts have been made to account for the mechanism of the Boson peak. Some researchers believe its origin is related to some kind of localized vibrations, but the physical explanation is still unclear. It may be possible to relate our study to the origin of the Boson peak, since the peak we found in this study may find in a wide class of systems with the strong and long-time correlated noise. While the Boson peak was observed in one-dimensional spectroscopy, multi-dimensional spectra presented in this study may give an additional insight into determining the mechanism [11,18,19].

Acknowledgements

We wish to thank Du Side for useful discussions. We thank financial support of a Grant-in-Aid for

Scientific Research (B) (12440171) from Japan Society for the Promotion of Science.

References

[1] H. Grabert, P. Schramm, G.-L. Ingold, Phys. Rep. 168 (1988) 115.
[2] U. Weiss, Quantum Dissipative Systems, second edn., World Scientific, Singapore, 1999.
[3] P. Talkner, P. Hänggi (Eds.), New Trends in Kramers' Reaction Rate Theory, Kluwer, Dordrecht, 1995.
[4] Y. Tanimura, R. Kubo, J. Phys. Soc. Jpn. 68 (1989) 101.
[5] S. Mukamel, Principle of Nonlinear Optical Spectroscopy, Oxford, New York, 1995.
[6] D.A. Blank, L.J. Kaufman, G. Fleming, J. Chem. Phys. 113 (2000) 771.
[7] L.J. Kaufman, D.A. Blank, G. Fleming, J. Chem. Phys. 114 (2001) 2312.
[8] M. Berg, D. Vanden Bout, Acc. Chem. Res. 30 (1997) 65.
[9] P. Hamm, M. Lim, W.F. DeGrado, R.M. Hochstrasser, Proc. Natl. Acad. Sci. USA 96 (1999) 2036.
[10] A. Tokmakoff, M.D. Fayer, Acc. Chem. Res. 28 (1995) 437.
[11] Y. Tanimura, S. Mukamel, J. Chem. Phys. 99 (1993) 9496.
[12] M. Cho, K. Okumura, Y. Tanimura, J. Chem. Phys. 108 (1998) 1326.
[13] Y. Suzuki, Y. Tanimura (in preprint).
[14] T. Kato, Y. Tanimura (in preprint).
[15] W.A. Philips (Ed.), Amorphous Solids: Low Temperature Properties, Springer, Berlin, 1981.
[16] O. Yamamuro, T. Matsuo, K. Takeda, T. Kanaya, T. Kawaguchi, K. Kaji, J. Chem. Phys. 105 (1996) 732.
[17] V.K. Malinovsky, V.N. Novikov, P.P. Parshin, A.P. Sokolov, M.G. Zemilanov, Europhys. Lett. 11 (1990) 43.
[18] K. Okumura, Y. Tanimura, J. Chem. Phys. 106 (1997) 1687;
J. Chem. Phys. 107 (1997) 2267;
Chem. Phys. Lett. 277 (1997) 159.
[19] R.A. Denny, D.R. Reichman, Phys. Rev. E 63 (2001) 065101.